Microwave and Millimeter-Wave Radiometric and Radiosonde Observations in an Arctic Environment

V. MATTIOLI

Dipartimento di Ingegneria Elettronica e dell'Informazione, Università di Perugia, Perugia, Italy

E. R. WESTWATER

Center for Environmental Technology, Department of Electrical and Computer Engineering, University of Colorado, Boulder, Colorado

D. CIMINI

CETEMPS, University of L'Aquila, L'Aquila, Italy

A. J. GASIEWSKI, M. KLEIN, AND V. Y. LEUSKI

Center for Environmental Technology, Department of Electrical and Computer Engineering, University of Colorado, Boulder, Colorado

(Manuscript received 5 October 2007, in final form 7 March 2008)

ABSTRACT

In a recent paper by Mattioli et al., a significant difference was observed between upper-tropospheric and lower-stratospheric water vapor profiles as observed by two radiosonde systems operating in the Arctic. The first was the Vaisala RS90 system as operated by the U.S. Department of Energy's Atmospheric Radiation Measurement Program; the second was the operational radiosondes launched by the U.S. National Weather Service that used the Sippican VIZ-B2 type. Observations of precipitable water vapor by ground-based microwave radiometers and GPS did not reveal these differences. However, both the microwave radiometer profiler (MWRP) and the ground-based scanning radiometer (GSR) contain channels that receive a significant response from the upper-tropospheric region. In this paper, it is shown that brightness temperature (T_b) observations from these instruments are in consistent agreement with calculations based on the RS90 data but differ by several degrees with calculations based on the VIZ radiosondes. It is also shown that calculations of T_b can serve as a gross quality control of upper-tropospheric soundings.

1. Introduction

In a recent paper (Mattioli et al. 2007), comparisons between remote and in situ measurements of water vapor during the 2004 North Slope of Alaska Arctic Winter Radiometric Experiment (NSA2004) were presented. The experiment was conducted for a 1-month period at the U.S. Department of Energy's Atmospheric Radiation Measurement (ARM) Program (Ackerman and Stokes 2003) field site near Barrow, Alaska. A complete description of the instruments used is given by Mattioli et al. (2007, and references therein). Most of the emphasis of the work was on tropospheric water vapor and the comparison of various measurement systems, both in situ and remote. However, there were some significant differences between the in situ systems in the upper troposphere and lower stratosphere, and these differences would be difficult to resolve by the two standard remote sounding systems of precipitable water vapor (PWV), namely the dual-frequency microwave radiometer (MWR) and the global positioning system (GPS). Two other sounders that were operated during NSA2004, the 12-channel microwave radiometer profiler (MWRP) and the 27-channel ground-based scanning radiometer (GSR) (Cimini et al. 2007a) can also measure PWV.

Corresponding author address: Vinia Mattioli, DIEI, Università di Perugia, via G. Duranti 93, 06125 Perugia, Italy.
E-mail: vinia.mattioli@diei.unipg.it

DOI: 10.1175/2008JTECHA1078.1

Moreover, the MWRP contains a channel at 22.235 GHz that is sensitive to upper-level water vapor (Deuber et al. 2004) and hence might give an independent confirmation of the differences between the various radiosonde systems. In addition, the GSR contains channels that are also sensitive to stratospheric water vapor (Cimini et al. 2007a,b). In this paper, before introducing our data, we give a short summary of the Mattioli et al. (2007) paper. We then present a weighting function analysis of various water vapor channels, explain a few details of our calculations, and, finally, discuss our main results.

2. Summary of radiometer–radiosonde comparisons from NSA2004

One of the major goals of NSA2004 was to evaluate the performance of radiosondes and operational remote sensing systems during cold (0° to – 40°C) and dry (PWV $<$ 0.5 cm) conditions. This was motivated because of the necessity to develop accurate forward models of both infrared and millimeter-wavelength radiometers during these conditions. Previously, experience at the ARM Southern Great Plains Central Facility in Oklahoma (Revercomb et al. 2003) and also in the tropics (Westwater et al. 2003), has shown that MWRs can be used to check the quality of radiosondes and to scale radiosonde humidity profiles to be consistent with PWV derived from the MWR. However, for the Arctic winter conditions, with PWV frequently less than 0.3 cm and surface temperatures less than −35°C, it has been questioned whether MWRs have the required sensitivity to perform the necessary scaling and/or quality checks.

During NSA2004, radiosondes were released from three sites within 5 km of each other. The radiosonde types included a Vaisala RS90-A (http://www.vaisala.com), operated at the ARM Duplex (DPLX) and at the Great White (GW) site; a Sippican VIZ-B2 type (http://www.sippican.com), operated by the National Weather Service (NWS); and a "Snow White" chilled-mirror dewpoint hygrometer, manufactured by Meteolabor AG, Switzerland (http://www.meteolabor.ch). There were also measurements of PWV by three independent remote sensors: (i) the dual-frequency MWR, operated by ARM and manufactured by Radiometrics (http://www.radiometrics.com); (ii) the MWRP, also operated by ARM and manufactured by Radiometrics; and (iii) a SuomiNet (http://www.suominet.ucar.edu) GPS receiver (SG27). The main conclusions of Mattioli et al. (2007) can be summarized as follows:

1) Relative humidity measurements from the Sippican carbon hygristor, both of the VIZ-B2 of NWS (NWS-VIZ) and the Sippican GPS Mark II (MK2-CH) operated at the DPLX, showed an apparent bias with respect to the other instruments (VIZ being higher) above the troposphere, with an average bias of the order of 16%–20%. In terms of PWV, the VIZ differed from RS90-A radiosondes by about 20% relative to an average PWV of 0.3 cm. Similar conclusions have been made by Wang et al. (2003) and by Ferrare et al. (2004) for upper-tropospheric and lower-stratospheric measurements at midlatitudes.
2) In using the MWRP, the use of all five channels in the water vapor band provided very good agreement with the MWR, with 0.033 cm rms (11% relative to the mean PVW). The PWV retrieved from the MWRP by using two channels (22.235 and 30 GHz) provided PWV values with a slightly larger dispersion (0.042 cm rms), due to a less frequent sampling of each channel of the MWRP (5 min) with respect to the MWR (30 s).
3) Over sample sizes that ranged from about 1000 to 7000 data points, the average bias values of the GPS, MWR, and MWRP (five channel) PWV retrievals were close, with differences generally better than 9% of the mean PWV, and the slopes of regression lines were close to unity (0.98). The bias differences in PWV between the remote sensors and radiosondes were larger, ranging from 10% to 30% of the mean PWV. Slope differences ranged from 0.91 to 1.11.
4) Diurnal differences in PWV were found when comparing RS90 radiosonde data with three independent measurements: MWR, MWRP, and NWS-VIZ. These diurnal differences were, respectively, 0.025, 0.016, and 0.027 cm. Such differences, although in a different climatic regime, were also found by Miloshevich et al. (2006) and were attributed to heating of the RS90 humidity elements.

3. Weighting function analysis

A standard way of showing the response of a radiometer to profile variations in temperature, water vapor, and cloud liquid is through weighting functions (Westwater 1993). Thus, in terms of variations in brightness temperature (T_b) from an initial background or initial guess profile as a function of height h, we have

$$\delta T_b = \int_0^\infty dh(W_T \delta T + W_{\rho_V} \delta \rho_V + W_{\rho_C} \delta \rho_C), \quad (1)$$

where δT, $\delta \rho_V$, and $\delta \rho_C$ represent profile variations in temperature, water vapor density, and cloud liquid, re-

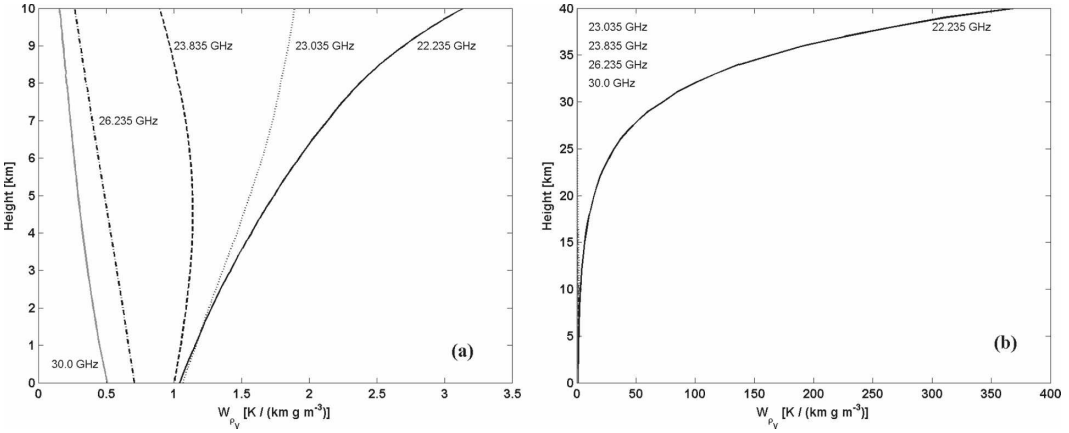

FIG. 1. Zenith water vapor density weighting functions calculated for the five channels of the MWRP for an average Arctic winter profile and a PWV of 1 mm. (a) Troposphere only. (b) Troposphere and stratosphere; note that the weighting functions for higher-frequency channels are not visible, as they remain on the order of 1 K (km g m^{-3})$^{-1}$.

spectively. Explicit formulas for calculating the weighting functions are given by Westwater (1993). Weighting function analyses for arctic atmospheres have been presented by Racette et al. (2005) and Cimini et al. (2007b).

a. MWRP weighting functions

The MWRP contains five K-band channels for sensing vapor and cloud liquid (22.235, 23.035, 23.835, 26.235, and 30.0 GHz). The weighting functions for the five K-band channels are shown in Fig. 1. Not shown are the two corresponding channels for the MWR. Figure 1a shows the tropospheric response to vapor. We note the nearly flat response of the 23.835-GHz channel, a good PWV channel, and the continued increase with height of the 22.235-GHz channel. This is amplified in Fig. 1b, where the response up to 40 km is shown. Note that the weighting functions for higher-frequency channels are not visible in this figure as they remain of the order of 1 K (km g m^{-3})$^{-1}$. In interpreting these weighting functions, it must be remembered that the contribution functions must be multiplied by the water vapor density to estimate the increment in T_b, and the water vapor roughly decreases exponentially with height. In addition, our calculations, using Eq. (1), have shown that the contributions to T_b from a change in temperature, for a fixed water vapor density, are negligible.

b. Ground-based scanning radiometer weighting functions

In addition to the ARM MWR and MWRP, during the experiment we also operated the 27-channel GSR, which measures T_b from 50 to 400 GHz (Cimini et al. 2007a). At low concentrations of water vapor, when stratospheric emission is not attenuated by the troposphere, channels near the line center are sensitive to water vapor in the stratosphere. In Fig. 2 we show weighting functions for three of the GSR channels distributed near the water vapor absorption line at 183.31 GHz. We note that the 183.31 $\pm$ 0.55, $\pm$1.0, and $\pm$3.05 GHz channels give a response to the water vapor at higher levels. Conversely, weighting functions for channels with frequency farther from line center (not shown) decay roughly exponentially with height.

4. Results

The MWRP and the MWR receivers are superheterodyne types with intermediate frequencies located 50–190 MHz on either side of the local oscillator frequencies. Since the bandpass (BP) filter characteristics are not available from the manufacturer, we calculated brightness temperatures with a couple of simple BP models: (i) average of lower and upper sidebands, assuming a rectangular BP; (ii) average of monochromatic centers of upper and lower sidebands; and (iii) the monochromatic center frequency. For the GSR, T_b calculations were performed using (i) the average of the BP as provided from the manufacturer and (ii) the average of monochromatic centers of upper and lower sidebands, while case (iii) is not applicable because of double-side BP filters. The results are shown in Table 1 for the RS90 radiosondes, in terms of average difference (avg), standard deviation (std), slope, intercept (int), and standard error (sde) of a linear fit. Confidence levels are also given. It can be noted that usually the calculations (i—iii) are within 0.01 K of each

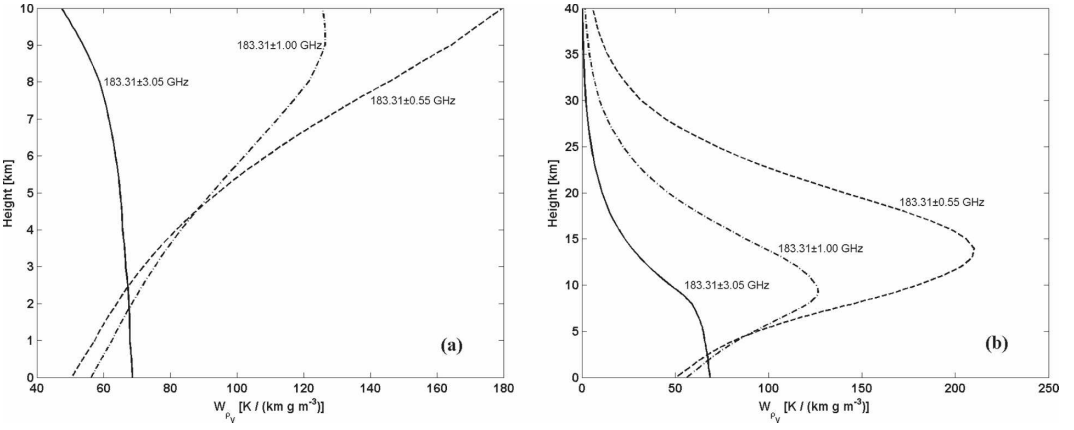

FIG. 2. Zenith water vapor density weighting functions for three water vapor channels of the GSR for an average Arctic winter profile and a PWV of 1 mm. (a) Troposphere only. (b) Troposphere and stratosphere.

other, while the agreement is of the order of 0.1–0.2 K for calculations at the 22.235- and 183-GHz channels. Our subsequent calculations are based on the calculations as in (i), that is, BP average. The results for the NWS-VIZ radiosondes are shown in Table 2, and clearly, except for channels at 22.235 and 183.31 GHz, the results are of similar quality to those shown in Table 1. The exception at the 22.235-GHz channel is due to the stratospheric response of the calculations at the center frequency. Differences between band-averaged and monochromatic calculations occur because of the 100-MHz gap around the centerline in the band averaging, which reduces the sensitivity to stratospheric or even mesospheric water vapor.

In Fig. 3, we show comparisons of time series of measured and calculated T_b for five of the MWRP channels and the two MWR channels, as well as for three channels of the GSR. For our calculations, we used the absorption model of Liljegren et al. (2005), which differs only slightly from the model of Clough et al. (2005). We notice the good agreement between the calculations and the measurements at all channels when the RS90 measurements are used, but, at times, substantial differences are evident when the NWS-VIZ radiosondes are used in the 22.235-GHz and the three GSR calculations.

In Fig. 4, we show the statistical results for the MWRP channel at which the departures are the most evident—the 22.235-GHz one that has a stratospheric response (Fig. 4a)—and the 23.835-GHz channel that only responds to tropospheric vapor (Fig. 4b). Figure 4b shows that T_b calculations at 23.835 GHz based on both RS90 and VIZ sondes are in good agreement with measurements, with bias and std values being less than 0.4 K. From Fig. 4b, we calculate that the rms's of VIZ and RS90 are 0.36 and 0.47 K, respectively. Similarly, in Fig. 4a, the comparisons between measurements and calculations for the RS90 show excellent agreement over a 16-K range in T_b with an rms difference of 0.4 K, a slope of 1.0, and an intercept of −0.29 K. Conversely, the comparison for the VIZ shows an rms difference of 2.6 K, a slope of 1.0, and an intercept of 1.91 K. Except for a few isolated points, there is a significant difference between MWRP measurements and calculations at 22.235 GHz based on VIZ soundings.

As shown in the papers by Cimini et al. (2007b) and Cadeddu et al. (2007), the response of the 183-GHz channels to water vapor is highly nonlinear, and channels near the line center will saturate for even modest amounts of water vapor. Nevertheless, at low amounts of PWV, say ≤2 mm, the channels at 183.31 ±0.55, ±1.0, and ±3.05 GHz can exhibit a stratospheric response. This response can be seen in Fig. 5, which shows scatterplots of the measured versus calculated T_bs for three GSR channels. The T_b measurements from the GSR were completely independent from the MWR and the MWRP, but again calculations from RS90 agree closely with T_b measurements, while calculations from VIZ radiosondes differed substantially. We note that the departures are consistent with the weighting functions shown in Fig. 2, that is, larger as the channel gets closer to the line center. In addition, the measurements tend to agree with calculations from the VIZ at higher T_bs, when saturation is becoming important, and the upper-atmospheric response is being attenuated. Differences of about 10 K in T_b calculations at 183.3 ± 1 GHz were found by Wang et al. (1995) when comparing AIR rawinsondes with the six-channel airborne millimeter-wave imaging radiometer (MIR; Racette et al. 1996).

We also investigated five cases in which there was apparent agreement between the MWRP T_b measure-

TABLE 1. Calculations minus MWRP measurement (K) based on the RS90 radiosondes (launched at both DPLX and GW) and the Liljegren et al. (2005) model. Clear skies only. Confidence levels are also given.

		Band averaged	Average of double-sideband mono	Center frequency
MWRP	Avg	−0.32 ± 0.05	−0.32 ± 0.05	−0.21 ± 0.05
22.235 GHz	Std	0.26 (0.23, 0.30)	0.26 (0.23, 0.30)	0.27 (0.24, 0.31)
N = 107	Int	−0.29 ± 0.19	−0.30 ± 0.19	−0.28 ± 0.20
	Slp	1.00 ± 0.02	1.00 ± 0.02	1.01 ± 0.02
	Sde	0.26 (0.23, 0.30)	0.26 (0.23, 0.30)	0.27 (0.24, 0.31)
MWRP	Avg	−0.35 ± 0.05	−0.35 ± 0.05	−0.34 ± 0.05
23.035 GHz	Std	0.25 (0.22, 0.29)	0.25 (0.22, 0.29)	0.25 (0.22, 0.29)
N = 107	Int	−0.58 ± 0.20	−0.58 ± 0.19	−0.59 ± 0.20
	Slp	1.02 ± 0.02	1.02 ± 0.02	1.02 ± 0.02
	Sde	0.24 (0.21, 0.28)	0.24 (0.21, 0.28)	0.24 (0.21, 0.28)
MWRP	Avg	−0.40 ± 0.05	−0.40 ± 0.05	−0.40 ± 0.05
23.835 GHz	Std	0.24 (0.21, 0.28)	0.24 (0.21, 0.28)	0.24 (0.21, 0.28)
N = 107	Int	−0.38 ± 0.23	−0.38 ± 0.23	−0.38 ± 0.23
	Slp	1.00 ± 0.02	1.00 ± 0.02	1.00 ± 0.02
	Sde	0.24 (0.21, 0.28)	0.24 (0.21, 0.28)	0.24 (0.21, 0.28)
MWR	Avg	−0.32 ± 0.04	−0.32 ± 0.04	−0.32 ± 0.04
23.8 GHz	Std	0.21 (0.18, 0.24)	0.21 (0.19, 0.24)	0.21 (0.19, 0.24)
N = 107	Int	−0.44 ± 0.18	−0.44 ± 0.18	−0.44 ± 0.18
	Slp	1.01 ± 0.02	1.01 ± 0.02	1.01 ± 0.02
	Sde	0.21 (0.18, 0.24)	0.21 (0.18, 0.24)	0.21 (0.18, 0.24)
MWRP	Avg	−0.59 ± 0.04	−0.59 ± 0.04	−0.59 ± 0.04
26.235 GHz	Std	0.22 (0.19, 0.25)	0.22 (0.19, 0.25)	0.22 (0.20, 0.26)
N = 107	Int	−0.43 ± 0.37	−0.43 ± 0.37	−0.42 ± 0.37
	Slp	0.98 ± 0.04	0.98 ± 0.04	0.98 ± 0.04
	Sde	0.22 (0.19, 0.25)	0.22 (0.19, 0.25)	0.22 (0.19, 0.25)
MWRP	Avg	−0.38 ± 0.05	−0.38 ± 0.05	−0.38 ± 0.05
30.0 GHz	Std	0.25 (0.22, 0.29)	0.25 (0.22, 0.29)	0.25 (0.22, 0.29)
N = 107	Int	−0.09 ± 0.77	−0.09 ± 0.77	−0.09 ± 0.77
	Slp	0.97 ± 0.07	0.97 ± 0.07	0.97 ± 0.07
	Sde	0.25 (0.22, 0.29)	0.25 (0.22, 0.29)	0.25 (0.22, 0.29)
MWR	Avg	−0.29 ± 0.04	−0.29 ± 0.04	−0.29 ± 0.04
31.4 GHz	Std	0.21 (0.19, 0.25)	0.21 (0.19, 0.25)	0.21 (0.19, 0.25)
N = 107	Int	0.28 ± 0.62	0.28 ± 0.62	0.28 ± 0.62
	Slp	0.95 ± 0.05	0.95 ± 0.05	0.95 ± 0.05
	Sde	0.21 (0.19, 0.25)	0.21 (0.19, 0.25)	0.21 (0.19, 0.25)
GSR	Avg	−0.45 ± 0.43	−0.35 ± 0.43	
183.31 ± 0.55 GHz	Std	2.22 (1.95, 2.57)	2.22 (1.95, 2.57)	
N = 103	Int	−0.35 ± 3.32	0.16 ± 3.32	
	Slp	1.00 ± 0.01	1.00 ± 0.01	
	Sde	2.23 (1.96, 2.58)	2.23 (1.96, 2.58)	
GSR	Avg	−0.18 ± 0.46	0.05 ± 0.46	
183.31 ± 1.0 GHz	Std	2.36 (2.07, 2.73)	2.34 (2.06, 2.72)	
N = 103	Int	−2.42 ± 3.11	−1.62 ± 3.10	
	Slp	1.01 ± 0.01	1.01 ± 0.01	
	Sde	2.34 (2.06, 2.72)	2.34 (2.06, 2.72)	
GSR	Avg	1.02 ± 0.59	1.34 ± 0.60	
183.31 ± 3.05 GHz	Std	3.00 (2.64, 3.48)	3.04 (2.68, 3.53)	
N = 103	Int	0.05 ± 2.21	−0.49 ± 2.22	
	Slp	1.01 ± 0.01	1.01 ± 0.01	
	Sde	3.01 (2.64, 3.49)	3.02 (2.65, 3.50)	

ments and the calculations of 22.235-GHz T_b from the VIZ soundings. The cases are highlighted in Fig. 6, in which the five soundings of agreement better than 0.5 K are labeled with letter A–E. Plots of the individual soundings, both by the VIZ and the Vaisala RS90, are shown in Fig. 7. Except for sounding B, all of the remaining cases have upper-altitude moisture from VIZ that is sensibly larger than that indicated by the RS90 soundings. What has happened is that the lower-tropospheric moisture from the VIZ sounding is low

TABLE 2. Calculations minus MWRP measurement (K) based on the NWS-VIZ radiosondes and the Liljegren et al. (2005) model. Clear skies only.

		Band averaged	Average of double-sideband mono	Center frequency
MWRP	Avg	1.94 ± 0.59	1.75 ± 0.53	6.77 ± 2.23
22.235 GHz	Std	1.68 (1.35, 2.22)	1.50 (1.20, 1.98)	6.28 (5.05, 8.31)
$N = 33$	Int	1.91 ± 2.85	1.83 ± 2.54	3.37 ± 10.59
	Slp	1.00 ± 0.20	0.99 ± 0.23	1.31 ± 0.95
	Sde	1.70 (1.37, 2.26)	1.52 (1.22, 2.02)	6.34 (5.08, 8.42)
MWRP	Avg	0.20 ± 0.17	0.20 ± 0.17	0.20 ± 0.17
23.035 GHz	Std	0.49 (0.40, 0.65)	0.49 (0.40, 0.65)	0.49 (0.40, 0.65)
$N = 33$	Int	−0.09 ± 0.91	−0.10 ± 0.90	−0.12 ± 0.90
	Slp	1.03 ± 0.08	1.03 ± 0.08	1.03 ± 0.08
	Sde	0.50 (0.40, 0.66)	0.50 (0.40, 0.66)	0.50 (0.40, 0.66)
MWR	Avg	0.11 ± 0.13	0.11 ± 0.13	0.10 ± 0.13
23.8 GHz	Std	0.36 (0.29, 0.48)	0.36 (0.29, 0.48)	0.36 (0.29, 0.48)
$N = 32$	Int	0.21 ± 0.58	0.21 ± 0.58	0.21 ± 0.58
	Slp	0.99 ± 0.05	0.99 ± 0.05	0.99 ± 0.05
	Sde	0.37 (0.29, 0.49)	0.37 (0.29, 0.49)	0.37 (0.29, 0.49)
MWRP	Avg	0.02 ± 0.13	0.02 ± 0.13	0.02 ± 0.13
23.835 GHz	Std	0.36 (0.29, 0.48)	0.36 (0.29, 0.48)	0.36 (0.29, 0.48)
$N = 33$	Int	−0.16 ± 0.78	−0.16 ± 0.78	−0.16 ± 0.78
	Slp	1.02 ± 0.07	1.02 ± 0.07	1.02 ± 0.07
	Sde	0.37 (0.30, 0.49)	0.37 (0.30, 0.49)	0.37 (0.30, 0.49)
MWRP	Avg	−0.38 ± 0.10	−0.38 ± 0.10	−0.38 ± 0.10
26.235 GHz	Std	0.27 (0.22, 0.36)	0.27 (0.22, 0.36)	0.27 (0.22, 0.35)
$N = 33$	Int	−0.41 ± 1.12	−0.41 ± 1.12	−0.41 ± 1.12
	Slp	1.00 ± 0.11	1.00 ± 0.11	1.00 ± 0.11
	Sde	0.28 (0.22, 0.37)	0.28 (0.22, 0.37)	0.28 (0.22, 0.37)
MWRP	Avg	−0.31 ± 0.09	−0.31 ± 0.09	−0.31 ± 0.09
30.0 GHz	Std	0.25 (0.20, 0.33)	0.25 (0.20, 0.33)	0.25 (0.20, 0.33)
$N = 33$	Int	0.73 ± 1.70	0.73 ± 1.70	0.73 ± 1.70
	Slp	0.91 ± 0.15	0.91 ± 0.15	0.91 ± 0.15
	Sde	0.25 (0.20, 0.33)	0.25 (0.20, 0.33)	0.25 (0.20, 0.33)
MWR	Avg	−0.12 ± 0.07	−0.12 ± 0.07	−0.12 ± 0.07
31.4 GHz	Std	0.20 (0.16, 0.27)	0.20 (0.16, 0.27)	0.20 (0.16, 0.27)
$N = 32$	Int	0.71 ± 1.06	0.71 ± 1.06	0.71 ± 1.06
	Slp	0.93 ± 0.09	0.93 ± 0.09	0.93 ± 0.09
	Sde	0.20 (0.16, 0.27)	0.20 (0.16, 0.27)	0.20 (0.16, 0.27)
GSR	Avg	13.71 ± 5.41	13.77 ± 5.42	
183.31 ± 0.55 GHz	Std	15.27 (12.28, 20.19)	15.29 (12.29, 20.22)	
$N = 33$	Int	107.97 ± 18.53	108.16 ± 18.5	
	Slp	0.58 ± 0.08	0.58 ± 0.08	
	Sde	7.28 (5.84, 9.68)	7.29 (5.84, 9.69)	
GSR	Avg	12.38 ± 4.72	12.56 ± 4.73	
183.31 ± 1.0 GHz	Std	13.30 (10.70, 17.60)	13.34 (10.73, 17.65)	
$N = 33$	Int	78.72 ± 18.50	79.19 ± 18.50	
	Slp	0.70 ± 0.08	0.70 ± 0.08	
	Sde	8.12 (6.51, 10.80)	8.13 (6.52, 10.80)	
GSR	Avg	13.25 ± 4.34	13.56 ± 4.32	
183.31 ± 3.05 GHz	Std	12.23 (9.84, 16.18)	12.17 (9.79, 16.10)	
$N = 33$	Int	33.94 ± 13.74	33.54 ± 13.80	
	Slp	0.88 ± 0.08	0.88 ± 0.08	
	Sde	10.78 (8.64, 14.33)	10.83 (8.68, 14.39)	

with respect to the RS90 and largely compensates for the upper-atmospheric excess. Thus, by itself, the 22.235-GHz channel does not give unambiguous proof of an incorrect sounding. However, the other four channels of the MWRP are mostly sensitive to lower-tropospheric vapor (see Fig. 1). We therefore developed a regression-based method to supplement the radiosonde quality check based on the single-frequency T_b measurements only. First we developed a training set of RS90 soundings that were taken since 2002 at the

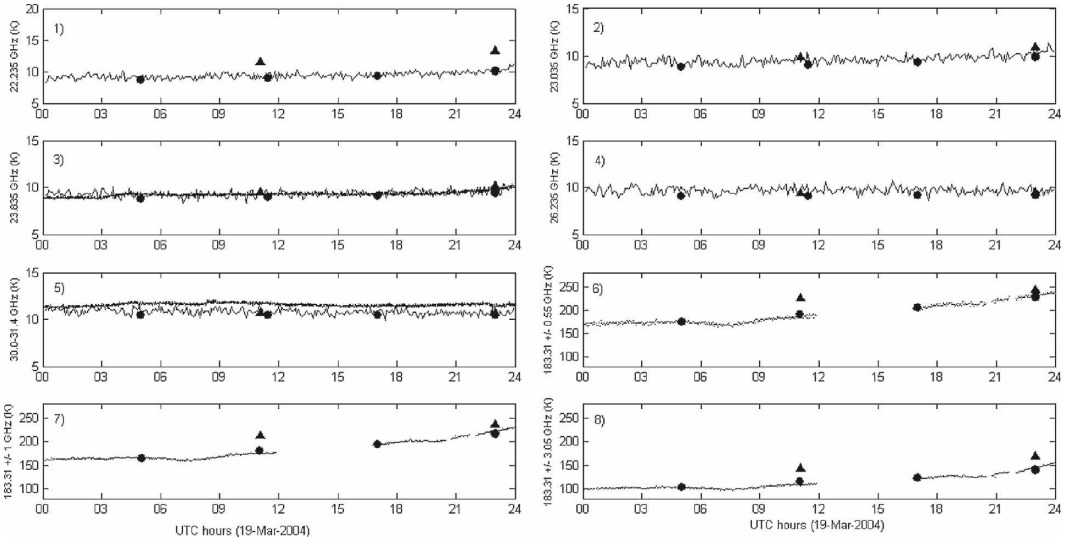

FIG. 3. Time series of data taken on 19 Mar 2004, showing T_bs at (1)–(5) five of the MWRP channels, (3), (5) (black lines) the two MWR channels, and (6)–(8) three of the GSR channels. The MWRP and MWR calculations used the absorption model of Liljegren et al. (2005) and band-averaged T_b calculations (based on the average of lower and upper sidebands, assuming a rectangular bandpass) for both RS90 and NWS-VIZ radiosondes. The GSR calculations were based on the bandpass functions of the manufacturer. Black triangles: T_b calculations using NWS-VIZ radiosondes. Black circles: T_b calculations using Vaisala RS90 radiosondes.

ARM Barrow site. Since many of these data had a variety of errors embedded within them, several of the original soundings were discarded after application of quality checks. Then, from the training set, we calculated band-averaged T_bs, as described in section 4, added Gaussian noise of 0.3-K rms to all of the T_bs, and then developed regression coefficients to estimate T_b at 22.235 GHz from a linear combination of the remaining four T_bs (23.035–30.0 GHz). We then applied these coefficients to the band-averaged T_bs calculated from NWS-VIZ at the MWRP four upper channels and compared them with the MWRP measurements at 22.235 GHz. Results are shown in Fig. 8. Here the original calculated versus measured pairs (as in Fig. 6) and the regression-estimated versus measured pairs are shown in black open and solid triangles, respectively.

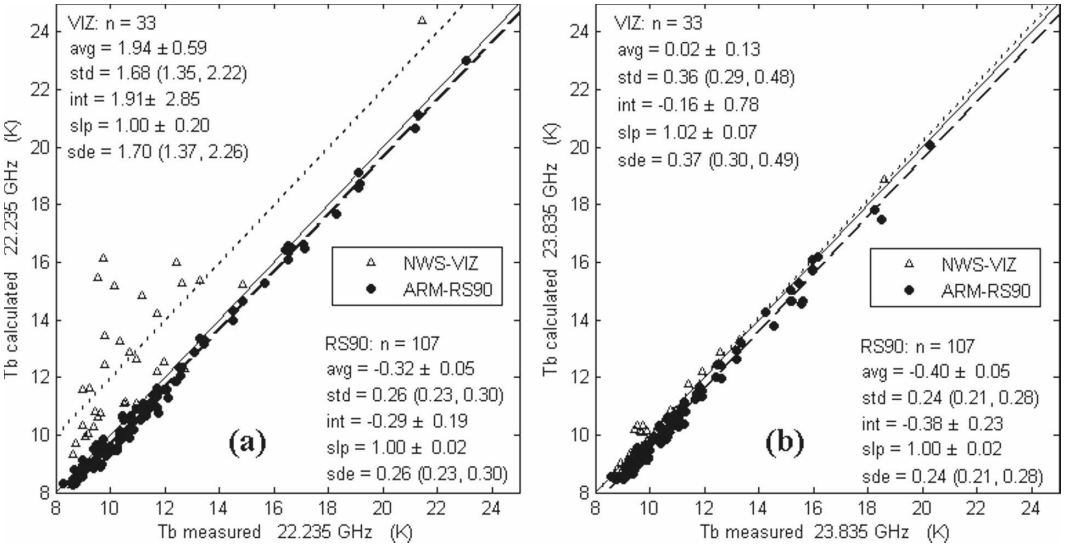

FIG. 4. Scatterplots of differences between calculations and MWRP measurements at (a) 22.235 and (b) 23.835 GHz. All statistical quantities refer to calculated − measured. Avg, std, int, and sde are in kelvins (K).

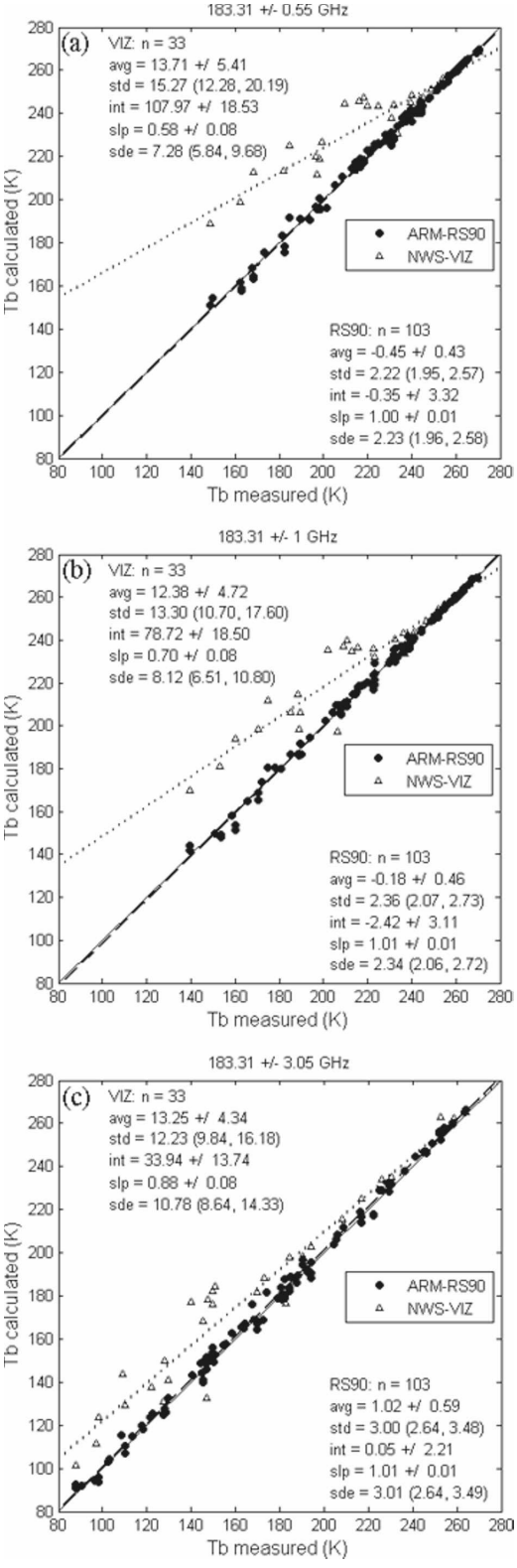

FIG. 5. Scatterplots of differences between calculations and GSR measurements at (a) 183.31 ± 0.5, (b) 183.31 ± 1, and (c) 183.31 ± 3.05 GHz. All statistical quantities refer to calculated – measured. Avg, std, int, and sde are in kelvins (K).

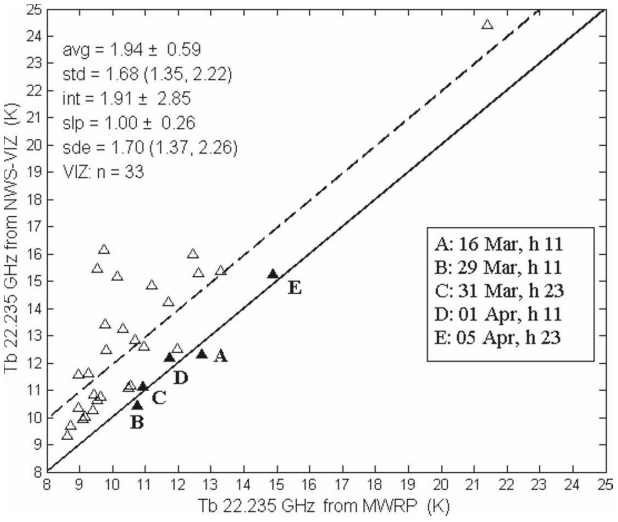

FIG. 6. Scatterplot of MWRP-measured T_b at 22.235 GHz vs T_b calculated from NWS-VIZ soundings. Clear-sky conditions. The letters A–E indicate soundings for which measured and calculated T_bs agree within 0.5 K. All statistical quantities refer to calculated – measured. Avg, std, int, and sde are in kelvins (K).

Both visually on a point-to-point basis and statistically, the overestimation of stratospheric water vapor is indicated reliably.

As a final comment, to make this quality check completely independent of the MWRP, one could estimate 22.235-GHz T_b from the higher-frequency T_bs computed from the NWS-VIZ. If T_b(calculated) − T_b(estimated) is larger than a predetermined threshold, then the sounding was probably affected by an upper-atmosphere bias. The potential interest on this quality check may be large since it does not require an independent instrument measurement (MWRP or GSR) to be performed. However, this approach is probably unable to detect cases such as A–E, described earlier (Figs. 6, 7).

5. Discussion

The measurements of the 22.235-GHz T_b were in close agreement with calculations based on the RS90 radiosondes, with an rms difference of 0.4 K. Conversely, similar comparisons with the VIZ radiosondes were, except for a few isolated points, significantly colder than the calculations. Thus, the 22.235-GHz measurements are in excellent agreement with the trends shown in the Mattioli et al. (2007) paper, in which the relative humidity measurements from the VIZ carbon hygristor (both the NWS-VIZ and the MK2-CH) show an apparent bias with respect to the other instruments above the troposphere, with an average bias of the order of 16%–20%.

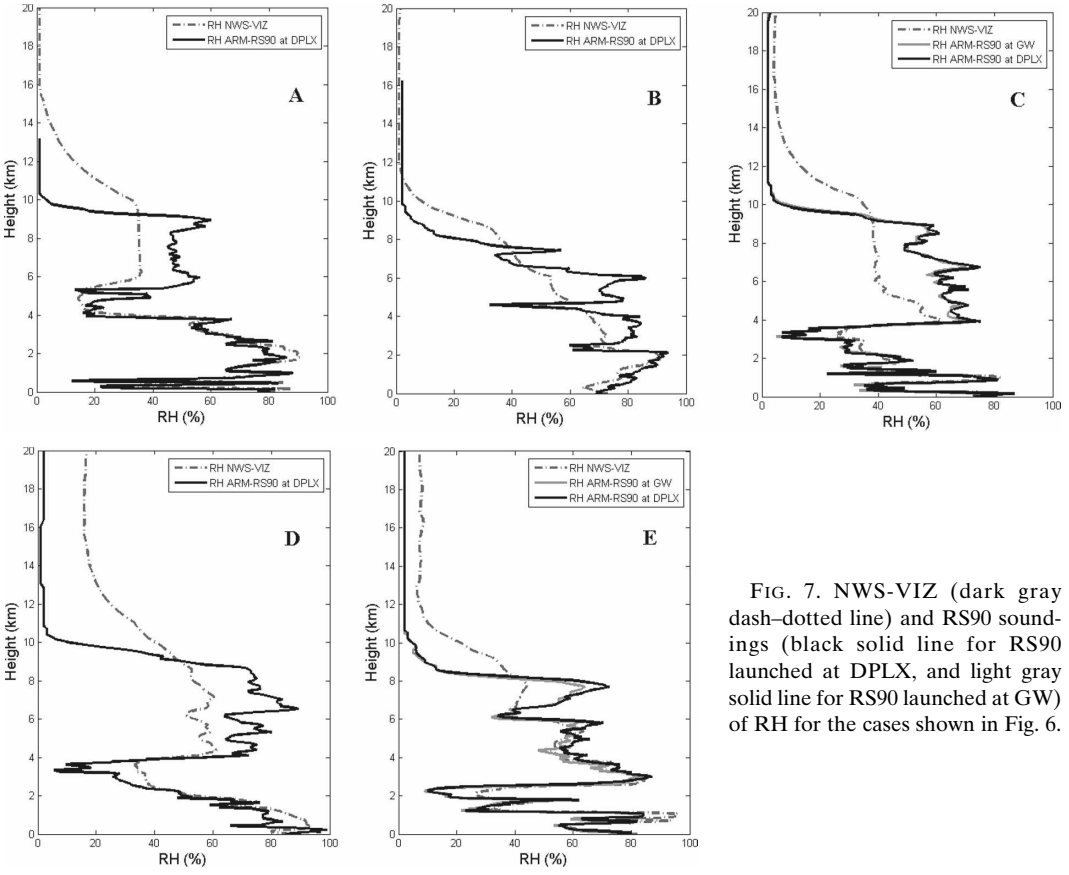

FIG. 7. NWS-VIZ (dark gray dash–dotted line) and RS90 soundings (black solid line for RS90 launched at DPLX, and light gray solid line for RS90 launched at GW) of RH for the cases shown in Fig. 6.

Occasionally, there were cases when T_b calculations at 22.235 GHz agreed with the MWRP measurements, although inspection of the associated soundings indicated there still was a problem with the upper-atmospheric VIZ sounding. This occurred in the cases when the NWS-VIZ sounding underestimated the tropospheric water vapor. To identify these cases, we developed a regression-based method, based on the four remaining channels, to identify mistaken cases. Every one of the cases showed a measured T_b that was larger, sometimes by as much as 6 K, than the estimated ones.

The independent measurements from the GSR support these findings. In fact, the GSR measurements showed substantial differences, as much as 30–40 K, from calculations based on the VIZ during low humidity. In the cold Arctic winter cases, say for PWV < 2 mm, GSR millimeter-wave observations represent another powerful method to identify spurious soundings.

It is intriguing to speculate on possible uses of the 22.235-GHz T_b and 183.31-GHz measurements to correct radiosonde soundings in the stratosphere. If a suitable training set of simultaneous RS90, NWS-VIZ, GSR, and MWRP observations were available, perhaps a correction could be derived and applied to both past and present soundings. At the ARM Barrow site, the MWRP has been operating since February 2004, and radiometers near 183.31 GHz are now operating on a continuous basis. Unfortunately, the ARM soundings, now using the Vaisala RS92 package, are launched at different times than the synoptic NWS soundings. A suitable set of simultaneous launches could potentially lead to a correction of the >10 yr NWS radiosonde climate record in Barrow, which may be important for the Arctic climate study.

The method presented here was based on forward model considerations only and for clear skies. Although we have not shown it here, the method could be extended to cover the cloudy-sky cases by deriving equivalent clear-sky T_b from the set of cloud-contaminated T_bs.

The MWRP and GSR instruments are only available for a few locations and dates, but the method of comparing calculations of near-resonant T_bs (e.g., 22.235 or 183.31 GHz), with those estimated from calculated T_bs that are only sensitive to lower-tropospheric vapor, could provide an independent quality check on stratospheric humidity sounding.

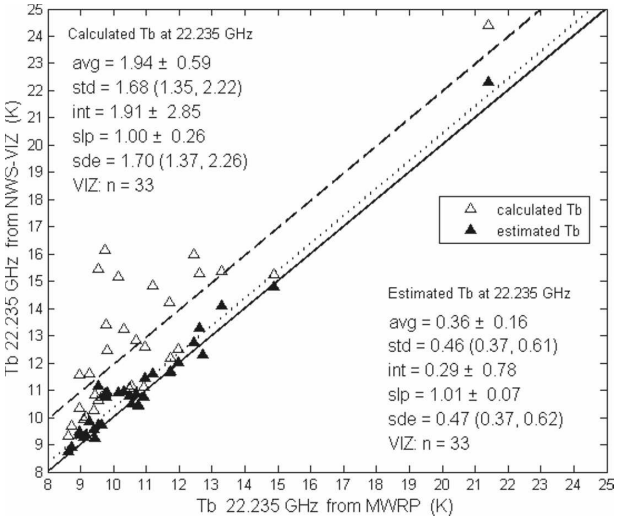

FIG. 8. Scatterplot of calculated and estimated T_bs at 22.235 GHz from the VIZ soundings (y axis) vs T_bs at 22.235 GHz measured by the MWRP. The comparison of the MWRP-measured T_bs at 22.235 GHz with the original T_b calculations from the VIZ sondes as in Fig. 6 are shown with white triangles. The comparison of the MWRP-measured T_bs at 22.235 GHz with the T_bs at 22.235 GHz estimated from the NWS- VIZ simulations at the upper-four channels of the MWRP are shown with black triangles. All statistical quantities refer to calculated – measured. Avg, std, int, and sde are in kelvins (K).

Acknowledgments. The work presented in this paper was sponsored by the Environmental Sciences Division of the Department of Energy under the Atmospheric Radiation Measurement Program.

REFERENCES

Ackerman, T. P., and G. M. Stokes, 2003: The Atmospheric Radiation Measurement Program. *Phys. Today,* **56,** 38–45.

Cadeddu, M. P., J. C. Liljegren, and A. L. Pazmany, 2007: Measurements and retrievals from a new 183-GHz water-vapor radiometer in the Arctic. *IEEE Trans. Geosci. Remote Sens.,* **45,** 2207–2215.

Cimini, D., E. R. Westwater, A. J. Gasiewski, M. Klein, V. Leuski, and S. Dowlatshahi, 2007a: The Ground-Based Scanning Radiometer (GSR): A powerful tool for the study of the Arctic atmosphere. *IEEE Trans. Geosci. Remote Sens.,* **45,** 2759–2777.

——, ——, ——, ——, ——, and J. C. Liljegren, 2007b: Ground-based millimeter- and submillimeter-wave observations of low vapor and liquid water contents. *IEEE Trans. Geosci. Remote Sens.,* **45,** 2169–2180.

Clough, S. A., M. W. Shepard, E. J. Mlawer, J. S. Delamere, M. J. Iacono, K. Cady-Pereira, S.-A. Boukabara, and P. D. Brown, 2005: Atmospheric radiative transfer modeling: A summary of the AER codes. *J. Quant. Spectrosc. Radiat. Transfer,* **91,** 233–244.

Deuber, B., N. Kämpfer, and D. G. Feist, 2004: A new 22-GHz radiometer for middle atmosphere water vapor profile measurements. *IEEE Trans. Geosci. Remote Sens.,* **42,** 974–984.

Ferrare, R. A., and Coauthors, 2004: Characterization of upper-troposphere water vapor measurements during AFWEX using LASE. *J. Atmos. Oceanic Technol.,* **21,** 1790–1808.

Liljegren, J. C., S.-A. Boukabara, K. Cady-Pereira, and S. A. Clough, 2005: The effect of the half-width of the 22-GHz water vapor line on retrievals of temperature and water vapor profiles with a twelve-channel microwave radiometer. *IEEE Trans. Geosci. Remote Sens.,* **43,** 1102–1108.

Mattioli, V., E. R. Westwater, D. Cimini, J. S. Liljegren, B. M. Lesht, S. I. Gutman, and F. J. Schmidlin, 2007: Analysis of radiosonde and ground-based remotely sensed PWV data from the 2004 north slope of Alaska Arctic Winter Radiometric Experiment. *J. Atmos. Oceanic Technol.,* **24,** 415–431.

Miloshevich, L. M., H. Vömel, D. N. Whiteman, B. M. Lesht, F. J. Schmidlin, and F. Russo, 2006: Absolute accuracy of water vapor measurements from six operational radiosonde types launched during AWEX-G and implications for AIRS validation. *J. Geophys. Res.,* **111,** D09S10, doi:10.1029/2005JD006083.

Racette, P. E., R. F. Adler, A. J. Gasiewski, D. M. Jackson, J. R. Wang, and D. S. Zacharias, 1996: An airborne millimeter-wave imaging radiometer for cloud, precipitation, and water vapor studies. *J. Atmos. Oceanic. Technol.,* **13,** 610–619.

——, and Coauthors, 2005: Measurement of low amounts of precipitable water vapor using ground-based millimeterwave radiometry. *J. Atmos. Oceanic Technol.,* **22,** 317–337.

Revercomb, H. E., and Coauthors, 2003: The ARM program's water vapor intensive observation periods: Overview, initial accomplishments, and future challenges. *Bull. Amer. Meteor. Soc.,* **84,** 217–236.

Wang, J., D. J. Carlson, D. B. Parsons, T. F. Hock, D. Lauritsen, H. L. Cole, K. Beierle, and E. Chamberlain, 2003: Performance of operational radiosonde humidity sensors in direct comparison with a chilled mirror dew-point hygrometer and its climate implication. *Geophys. Res. Lett.,* **30,** 1860, doi:10.1029/2003GL016985.

Wang, J. R., S. H. Melfi, P. E. Racette, D. N. Whitemen, L. A. Chang, R. A. Ferrare, K. D. Evans, and F. J. Schmidlin, 1995: Simultaneous measurements of atmospheric water vapor with MIR, Raman lidar, and rawinsondes. *J. Appl. Meteor.,* **34,** 1595–1607.

Westwater, E. R., 1993: Ground-based microwave remote sensing of meteorological variables. *Atmospheric Remote Sensing by Microwave Radiometry,* M. A. Janssen, Ed., John Wiley & Sons, 145–213.

——, B. Stankov, D. Cimini, Y. Han, J. A. Shaw, B. M. Lescht, and C. N. Long, 2003: Radiosonde humidity soundings and microwave radiometers during Naura99. *J. Atmos. Oceanic Technol.,* **20,** 953–971.